Self-assembly and characterization of small and monodisperse dye nanospheres in a protein cage

Luque, Daniel; de la Escosura, Andres; Snijder, Joost; Brasch, Melanie; Burnley, Rebecca J.; Koay, Melissa S. T.; Carrascosa, Jose L.; Wuite, Gijs J. L.; Roos, Wouter H.; Heck, Albert J. R.

Published in:
Chemical Science

DOI:
10.1039/c3sc52276h

Publication date:
2013

Chemical Science

EDGE ARTICLE

View Article Online
View Journal | View Issue

Cite this: *Chem. Sci.*, 2014, **5**, 575

Self-assembly and characterization of small and monodisperse dye nanospheres in a protein cage†

Daniel Luque,[a] Andrés de la Escosura,*[b] Joost Snijder,[cde] Melanie Brasch,[f] Rebecca J. Burnley,[cd] Melissa S. T. Koay,[f] José L. Carrascosa,[a] Gijs J. L. Wuite,[e] Wouter H. Roos,[e] Albert J. R. Heck,[cd] Jeroen J. L. M. Cornelissen,*[f] Tomás Torres*[bg] and José R. Castón*[a]

Received 13th August 2013
Accepted 30th September 2013

DOI: 10.1039/c3sc52276h

www.rsc.org/chemicalscience

Phthalocyanines (Pc) are dyes in widespread use in materials science and nanotechnology, with numerous applications in medicine, photonics, electronics and energy conversion. With the aim to construct biohybrid materials, we here prepared and analyzed the structure of two Pc-loaded virus-like particles (VLP) with diameters of 20 and 28 nm (*i.e.*, $T = 1$ and $T = 3$ icosahedral symmetries, respectively). Our cryo-electron microscopy (cryo-EM) studies show an unprecedented, very high level of Pc molecule organization within both VLP. We found that 10 nm diameter nanospheres form inside the $T = 1$ VLP by self-assembly of supramolecular Pc stacks. Monodisperse, self-assembled organic dye nanospheres were not previously known, and are a consequence of capsid-imposed symmetry and size constraints. The Pc cargo also produces major changes in the protein cage structure and in the mechanical properties of the VLP. Pc-loaded VLP are potential photosensitizer/carrier systems in photodynamic therapy (PDT), for which their mechanical behaviour must be characterized. Many optoelectronic applications of Pc dyes, on the other hand, are dependent on dye organization at the nanoscale level. Our multidisciplinary study thus opens the way towards nanomedical and nanotechnological uses of these functional molecules.

Introduction

Organic dyes such as porphyrins and phthalocyanines (Pc) are among the most promising photoactive materials for applications ranging from photodynamic therapy to non-linear optics and organic photovoltaics.[1,2] Pc are chemically and thermally stable compounds that absorb in the red/near-infrared region (NIR) of the solar spectrum, with extinction coefficient values greater than 1×10^5 M^{-1} cm^{-1}.[3–5] The development of nanostructures from these dyes has attracted much attention in the field of materials science, mainly because the chemical, electronic and photophysical properties of the resulting nanosized aggregates differ from those of the isolated monomers.[6,7] Spherical nanoparticles composed solely of dye molecules have been prepared, usually by the so-called reprecipitation method,[8] which allows tuning of the optical properties of the dye through non-covalent interactions.[9–12] Nanoparticles obtained in this way are amorphous and polydisperse, with sizes ranging from 30 to 100 nm, which tend to agglomerate with time.

Virus capsids and protein cages are nanoplatforms that can be used for precise positioning of functional species,[13–16] at inner and/or outer surfaces,[17–20] or as nanocontainers to encapsulate different types of materials.[21–26] One of the most common capsids used for this purpose is that of the cowpea chlorotic mottle virus (CCMV). CCMV is a positive, single-strand RNA plant virus whose 28 nm diameter capsid comprises 90 coat protein (CP) dimers (180 total CP subunits, each composed of 190 amino acid residues) that form 12 pentameric and 20 hexameric capsomers in a $T = 3$ lattice.[27,28] Assembly of the CCMV capsid is a reversible process. At neutral pH and high ionic strength, the capsid disassembles into CP dimers. After removal of RNA, empty capsids of the same size and geometry as

[a]*Department of Structure of Macromolecules, Centro Nacional de Biotecnología/CSIC, Cantoblanco, 28049 Madrid, Spain. E-mail: jrcaston@cnb.csic.es; Fax: +34 91 585 4506; Tel: +34 91 585 4971*

[b]*Universidad Autónoma de Madrid, Organic Chemistry Department, Cantoblanco, 28049 Madrid, Spain. E-mail: andres.delaescosura@uam.es; Fax: +34 91 497 3966; Tel: +34 91 497 2773*

[c]*Biomolecular Mass Spectrometry and Proteomics Group, Bijvoet Center for Biomolecular Research and Utrecht Institute for Pharmaceutical Sciences, Utrecht University, Padualaan 8, 3584 CH Utrecht, The Netherlands*

[d]*Netherlands Proteomics Center, Padualaan 8, 3584 CH Utrecht, The Netherlands*

[e]*Natuur- en Sterrenkunde and LaserLab, Vrije Universiteit, De Boelelaan 1081, Amsterdam, The Netherlands*

[f]*Laboratory for Biomolecular Nanotechnology, MESA+ Institute for Nanotechnology, University of Twente, PO Box 217, 7500 AE Enschede, The Netherlands. E-mail: j.j.l.m.cornelissen@utwente.nl; Fax: +31 53 489 4645; Tel: +31 53 489 2980*

[g]*IMDEA-Nanociencia, Ciudad Universitaria de Cantoblanco, 28049 Madrid, Spain. E-mail: tomas.torres@uam.es; Fax: +34 91 497 3966; Tel: +34 91 497 4151*

† Electronic supplementary information (ESI) available: Detailed procedures for preparation of samples **1–4** and their complete characterization by SEC, MS, UV-Vis spectroscopy, cryo-EM and AFM. See DOI: 10.1039/c3sc52276h

the native virus can be reassembled if the pH is reduced to 5. This behavior has been used to encapsulate materials such as fluorescent proteins,[29] enzymes[30,31] and inorganic nanoparticles.[21,32] At neutral pH, CP assembly requires polyanionic templates such as negative micelles[33] and synthetic anionic polymers.[34–37] These templates produce an interesting assembly landscape of the CCMV CP[38] that, depending on medium conditions and cargo, can form a variety of structures such as tubes[39–41] and icosahedral capsids with $T = 1$ (containing 30 CP dimers), '$T = 2$' (60 dimers) and $T = 3$ (90 dimers) architecture.[42–44]

Although inorganic nanoparticles of various types and functions have been grown inside virus capsids and protein cages,[13–16] this approach has not been used to template production of purely self-assembled organic nanoparticles. Based on our study of Pc encapsulation in virus-like particles (VLP) as potential photosensitizer/vehicle systems for photodynamic therapy (PDT),[45] here we show the formation of small and monodisperse Pc nanoparticles inside a protein cage assembled from the CCMV CP (Fig. 1). The 20 and 28 nm VLP under study (with $T = 1$ and $T = 3$ symmetries, respectively) contain water-soluble tetrasulfonated zinc Pc (ZnPc), which forms supramolecular H-type dimers in aqueous solution by π–π and hydrophobic interactions.[46] Our cryo-electron microscopy three-dimensional reconstruction (cryo-EM 3DR) of the ZnPc-loaded $T = 1$ VLP indicates that at neutral pH, the 10 nm ZnPc nanospheres that form inside the protein cage, template the CP assembly. In turn, confinement within the cage determines the much smaller and completely monodisperse size of these ZnPc nanospheres compared to that of any other dye nanoparticle reported. The highly organized state of ZnPc molecules within these nanospheres, as shown by their intense electron density in the VLP cryo-EM map, explains their dye optical behavior after encapsulation. We also conducted atomic force microscopy (AFM) nanoindentation experiments, which showed that the mechanical properties of the protein cage are affected by the inner organic nanoparticle. These studies show a simple way to template self-assembly of small and monodisperse dye nanospheres, opening the way towards the use of these biohybrid materials for nanomedical and optoelectronic applications.

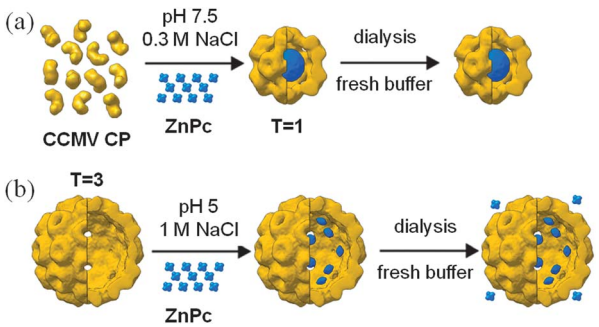

Fig. 1 (a) Self-assembly of 10 nm ZnPc nanospheres within a 20 nm ($T = 1$) protein cage formed by CCMV CP, as shown by cryo-EM 3DR of these VLP. (b) Encapsulation of ZnPc in $T = 3$ CCMV capsids, studied by the same technique. ZnPc structure is shown in Scheme S1, ESI.†

Results and discussion

Synthesis of ZnPc-loaded VLP

ZnPc-loaded $T = 1$ (sample **1**) and $T = 3$ (sample **2**) VLP were assembled by two routes (Fig. 1). Encapsulation of polyanionic species in CCMV-based VLP is driven by electrostatic interactions between the negative cargo (here, ZnPc) and positively charged residues from the CP.[39–45] As well as samples **1** and **2**, two additional samples were studied to establish precise comparisons between VLP properties with and without ZnPc; sample **3** consisted of empty $T = 3$ capsids obtained from full-length CP, and sample **4** contained capsid assemblies from truncated CP (*i.e.*, CP lacking residues 1–27/32; see below).

To prepare sample **1**, ZnPc and CP were incubated (at final concentrations of 3 and 0.35 mM, respectively) in Tris–HCl buffer (50 mM, 0.3 M NaCl, 1 mM dithiothreitol, pH 7.5) and purified by preparative size exclusion chromatography (SEC) (Fig. S1a, ESI†). This process yields stable ZnPc-loaded $T = 1$ VLP, although mass spectrometry (MS) analysis showed a small additional population that could represent ZnPc-loaded '$T = 2$' particles (Fig. 2a, top). The mass of the ZnPc-loaded $T = 1$ VLP was determined by tandem MS as 1.3 MDa, which indicates an

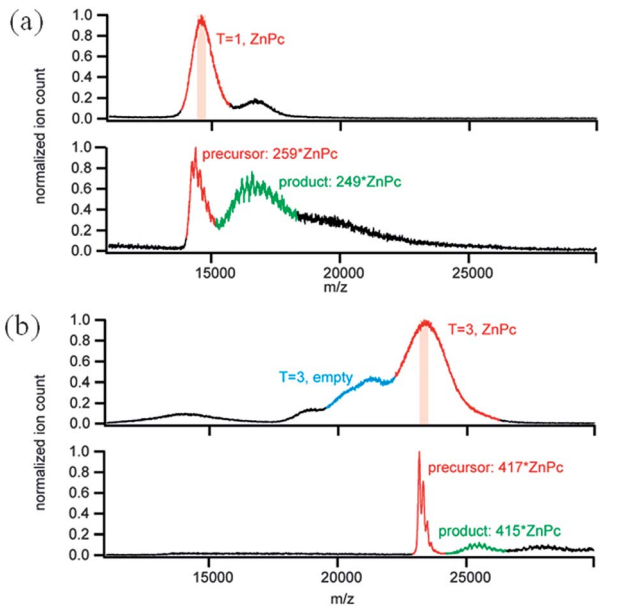

Fig. 2 MS spectra of ZnPc-loaded VLP. Top panels: native MS spectra; bottom panels: tandem MS analysis. Signals assigned to ZnPc-loaded VLP (red); empty VLP (blue). The additional signals are attributed to '$T = 2$' particles in (a) and aberrant structures in (b). (a) Estimate of ZnPc molecule number in $T = 1$ VLP (sample **1**) with tandem MS. The shaded area (top) was selected and dissociated (bottom), yielding ion resolved signals on both the precursor and the first dissociation product. The resulting masses from the ion resolved signals are 1340 ± 1.2 kDa and 1330 ± 1.2 kDa for precursor and product, respectively (mean ± standard deviation over all charge states). This corresponds to an average of 259 and 249 ZnPc molecules, respectively (details in Table S1, ESI†). (b) Estimate of ZnPc molecule number in $T = 3$ VLP (sample **2**). Masses of precursor and product are 3476 ± 0.7 kDa and 3444 ± 1.3 kDa, respectively, corresponding to 417 and 405 ZnPc molecules (details in Table S1, ESI†). The mass of ZnPc is 892 Da.

average of 250 ZnPc molecules per capsid (Fig. 2a, bottom). The lack of ion resolution on intact particles indicates substantial mass heterogeneity in the VLP, which is also clear from the relatively broad peaks observed in tandem MS analyses.

Sample **2** was prepared by incubation of ZnPc and empty $T = 3$ capsids (starting concentrations of 3 mM ZnPc and 0.35 mM CP) in sodium acetate buffer (50 mM, 1 M NaCl, 1 mM NaN_3, pH 5) and preparative SEC (Fig. S1b, ESI†). In these conditions, ZnPc molecules diffuse into the capsids through their pores, driven by electrostatic attractive interactions with positively charged residues on the CP inner surface. When sample **2** was dialyzed against fresh buffer, ZnPc diffused out of the capsids, suggesting that the encapsulation is an equilibrium process. MS analysis confirmed this observation; in addition to the major peak for ZnPc-loaded $T = 3$ VLP, we detected peaks for empty $T = 3$ capsids, as well as a small proportion of ZnPc-loaded $T = 1$/'$T = 2$' particles or aberrant structures (Fig. 2b, top). These data are in marked contrast with those obtained for control samples **3** and **4** (Fig. S2, ESI†). Using tandem MS, we determined the mass of the ZnPc-loaded $T = 3$ VLP as 3.5 MDa, which indicates an average of 400 ZnPc molecules per capsid (Fig. 2b, bottom).

We used MS data to obtain information regarding CP sequence composition in the VLP. Empty $T = 3$ capsids (sample **3**) were composed of full-length CP, whereas ZnPc-loaded $T = 1$ and $T = 3$ VLP contained mainly truncated CP (residues 28/33–190; Fig. S3, ESI†). This truncation in the ZnPc-loaded VLP could be due to prolonged incubation at pH 7.5 during sample handling. Extended incubation of disassembled CP at pH 7.5 (*i.e.*, sample **4**) led to near-complete truncation (Fig. S3, ESI† bottom), but ZnPc–CP interactions might also affect CP truncation.

The MS results indicated that the CP N terminus is not necessary to retain ZnPc in the VLP. We postulate that residues involved in CP–RNA interactions in the native virus (Glu34, Lys42, Lys45, Trp47, Thr48, Arg82, Lys87, Arg90, Glu140, Lys143, Arg179, Thr181 and Asp184; all present in ordered CP regions)[27] interact with ZnPc. The seven positively-charged residues (4 Lys, 3 Arg) might interact with the negatively-charged ZnPc sulfonate groups, and Thr, Glu and Asp residues could coordinate (*via* OH and COOH groups) the zinc metal center, whereas Trp47 might mediate aromatic interactions with the dye.

Structure of ZnPc-loaded VLP

To study the structure of ZnPc-loaded $T = 1$ and $T = 3$ VLP, using the empty $T = 3$ capsid as a reference, we analyzed samples **1**, **2** and **3** by cryo-EM. Electron micrographs of the particles and their 3DR are shown (Fig. 3 and S4, ESI†); particle dimensions are inferred from the radial density profiles from 3D maps (Fig. 4). For each VLP type, the majority of the particles were structurally homogeneous.

Cryo-EM analysis of empty $T = 3$ capsids. Sample **3** was formed by three populations of assembled particles (Fig. 3a and d). We observed two sizes of empty $T = 3$ capsids, termed A- (Fig. 3d, left) and B-capsids (Fig. 3d, center). The radial difference was small (14.0 and 14.2 nm, respectively; Fig. 4, red and black curves), but sufficiently large to obtain higher resolution 3DR maps than a single 3DR with mixed particles. A- and B-capsids made up 58% of total particles in the sample (28% A-capsids, 30% B-capsids). The presence of two particle sizes is probably due to CP conformational flexibility, and differs from dynamic swelling of the CCMV capsid, which produces larger size changes (*i.e.*, *ca.* 5%)[47] in comparison to the present case (*i.e.*, *ca.* 1%). The density for the characteristic β-annulus, due to CP N-terminal residues (29–33) at the threefold axes,[48] was detected only in B-capsids (Fig. 3d, arrows), which suggests an increase in order of the N termini in hexameric capsomers. In addition, 25.2 nm diameter particles were observed in sample **3** (Fig. 4, blue curve; 19% of total particles), from which we reconstructed the '$T = 2$' capsid map (Fig. 3d, right). The remaining particulate material in sample **3** (23% of total particles) was irregular or did not show icosahedral symmetry and was not included in any of the density maps.

Cryo-EM analysis of ZnPc-loaded $T = 3$ VLP. The 3DR of ZnPc-loaded $T = 3$ VLP (sample **2**) showed additional densities that cannot be ascribed to CP (Fig. 3e, blue). These extra densities must be due to ZnPc, and provided data on their location and organization within the protein cage. Capsid structure was almost identical to that of the $T = 3$ empty capsids, both in the large depression/pore size (Fig. 3e, top) and radius (14.6 nm; Fig. 4, green curve). In the capsid interior, the ZnPc density was beneath the hexamers, with no extra density in front of pentamers (Fig. 3e, bottom). The radial density plot showed ZnPc-related densities at a radius of 8.2 nm (Fig. 4, green arrow). The ZnPc location beneath hexameric capsomers is probably related to the greater order of CCMV CP positively charged residues in hexamers than in pentamers (see below).[48] Each of the encapsulated ZnPc dimers (as found in aqueous solution and within the $T = 3$ VLP) contains 8 negative charges that can interact with the 7 or 8 accessible, positively-charged CP residues. The densities for icosahedral ordered ZnPc account for only a fraction of the total encapsulated ZnPc molecules (an average of 400 ZnPc molecules as estimated by MS); a large number of ZnPc dimers in the capsid interior thus do not follow icosahedral symmetry (Fig. S5a, ESI†).

Cryo-EM analysis of ZnPc-loaded $T = 1$ VLP. The radius (10.2 nm; Fig. 4, yellow curve) and morphology of ZnPc-loaded $T = 1$ VLP (sample **1**) are consistent with the 60 CP subunit arrangement with $T = 1$ symmetry (Fig. 3f). There were nonetheless notable differences with the $T = 1$ capsids reported for a mutant CCMV protein (NΔ34, which lacks most of the N-terminal domain);[49] in the absence of a polyanionic template, this particle symmetry can only be obtained by such a mutation. The pores at threefold axes were much larger in ZnPc-loaded $T = 1$ VLP than in NΔ34 $T = 1$ capsids (Fig. 3f, top). We show that, in addition to the cargo effect on capsid structure, the capsid imposes organization on the ZnPc. The cryo-EM map indicated a conspicuous ZnPc density in the capsid interior (Fig. 3f, bottom, blue), with spherical morphology and a 5.2 nm radius (Fig. 4, yellow curve). To be detected, ZnPc molecules must be well organized within the spheres.

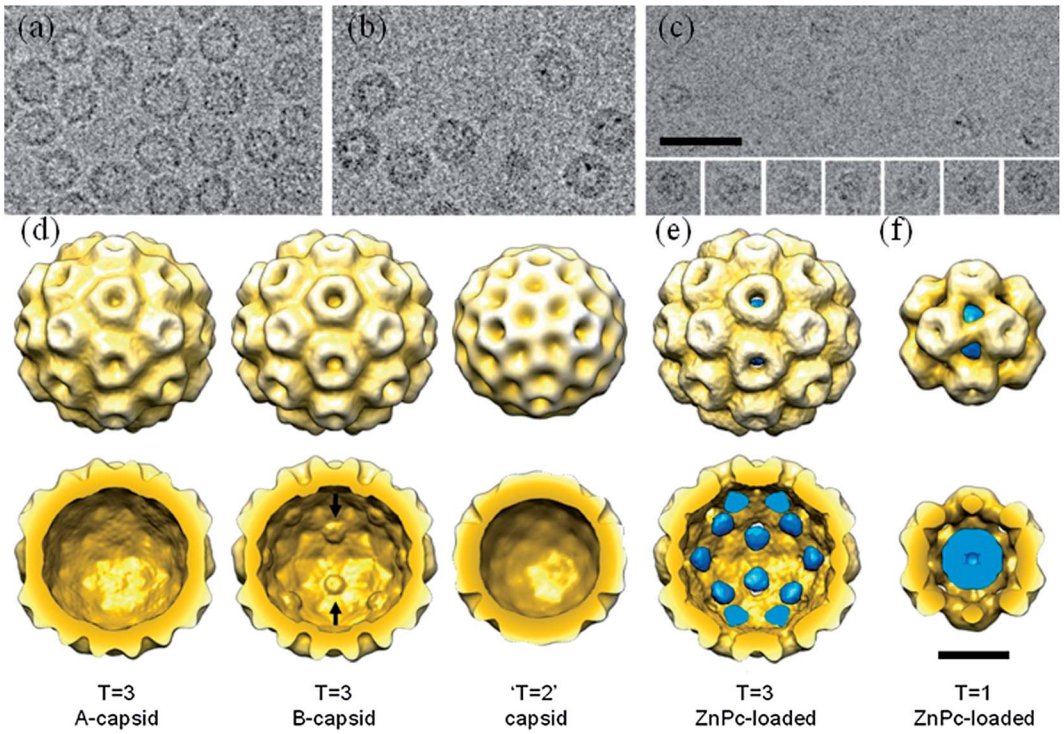

Fig. 3 Three-dimensional cryo-EM reconstructions of empty and ZnPc-loaded CCMV capsids. Cryo-EM of samples (a) **3**, (b) **2** and (c) **1**. Scale bar, 50 nm. (d–f) Surface-shaded representations of the outer (top row) and inner surfaces (bottom row), viewed along an icosahedral twofold axis : cryo-EM 3DR of the (d) A-capsid (diameter 28.0 nm), B-capsid (28.4 nm) and '$T = 2$' capsid (25.2 nm), all empty and present in sample **3**; (e) ZnPc-loaded $T = 3$ VLP (29.2 nm), in sample **2**; and (f) ZnPc-loaded $T = 1$ VLP (20.4 nm), in sample **1**. Scale bar, 10 nm.

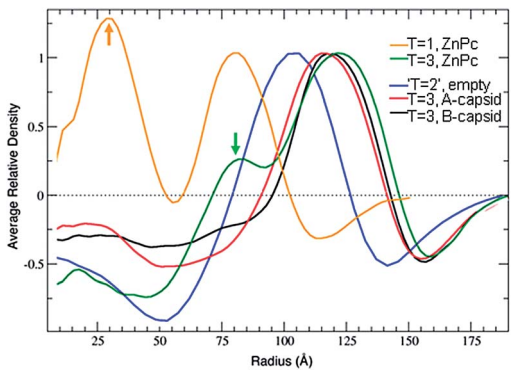

Fig. 4 Radial density profiles from 3D maps of the capsids.

Pseudo-atomic models of ZnPc-loaded VLP

Docking the CCMV capsid protein crystal structure (PDB 1CWP) into the cryo-EM density maps of ZnPc-loaded $T = 3$ and $T = 1$ VLP showed marked structural differences (Fig. 5).

For ZnPc-loaded $T = 3$ VLP, the ends of the hexameric CP N-terminal arms (at residue 28, the first non-truncated residue) were in close proximity and contacted the ZnPc density (Fig. 5a, left; yellow and green spheres for B and C subunits, respectively). The surface Coulomb potential on the inner capsid shell (Fig. 5a, right) showed that positively charged CP residues were also closer at threefold axes (*i.e.*, in hexameric capsomers) than at fivefold axes. This effect is necessarily related to ZnPc dimer binding by CP hexamers.

For ZnPc-loaded $T = 1$ VLP, the CP N-terminal arms (Fig. 5b, left) and positively charged residues (Fig. 5b, right) were distributed more distantly and homogeneously around the fivefold axes on the capsid interior surface. This pentameric CP subunit arrangement might be explained by the need to bind the spherical ZnPc cargo, leading in turn to much larger pores at threefold axes than those in NΔ34 $T = 1$ capsids.[49]

We analyzed the hinge angle formed between CP dimers in each VLP type. An earlier study of empty $T = 3$ capsids showed hinge dihedral angles of 38° for A–B (at quasi–twofold axes) and 42° for C–C dimers (at twofold axes), whereas the angle was 45° for CP dimers in $T = 1$ capsids assembled from the NΔ34 CP mutant.[49] In ZnPc-loaded $T = 3$ VLP, the hinge dihedral angles for A–B (Fig. 6a) and C–C dimers (Fig. 6b) were identical to those reported for the empty $T = 3$ capsid. In contrast, ZnPc-loaded $T = 1$ VLP CP dimers had a hinge dihedral angle of 62° (Fig. 6c), much larger than that of the NΔ34 $T = 1$ capsid. This large hinge dihedral angle resembles that found at the quasi-twofold axes of the swollen CCMV capsid.[50] We postulated that these differences in protein cage structure between ZnPc-loaded VLP might lead to distinct mechanical properties.

Mechanical properties of ZnPc-loaded VLP

The mechanical properties of virus capsids, as determined by AFM nanoindentation, are a physical signature of capsid stability and conformational dynamics.[51] To test the effect of ZnPc encapsulation on the stability of ZnPc-loaded VLP, we

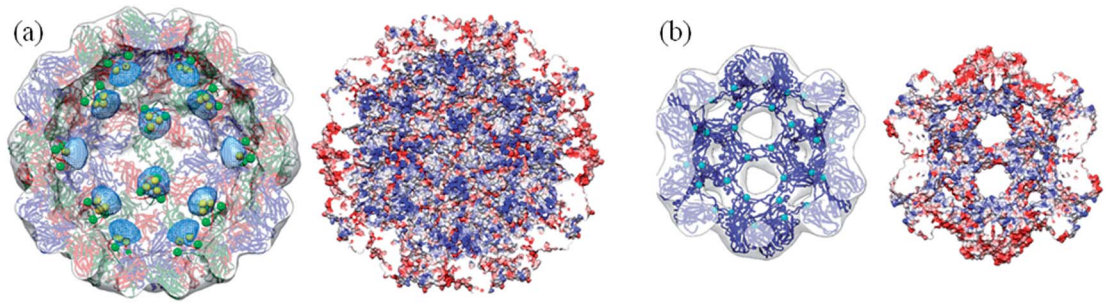

Fig. 5 Pseudo-atomic model of ZnPc-loaded $T = 3$ and $T = 1$ capsids. (a) $T = 3$ and (b) $T = 1$ capsid viewed down a twofold axis from inside, with docked CCMV protein atomic coordinates (left). The three types of CP subunits (A, B and C) are depicted in blue, red and green, respectively. B and C N termini converge at the threefold axis (the last visible N-terminal residue is indicated as a sphere). (a, b, right) As above, with electrostatic potentials shown for accessible inner surfaces, indicating negative (red) and positive (blue) charge distribution.

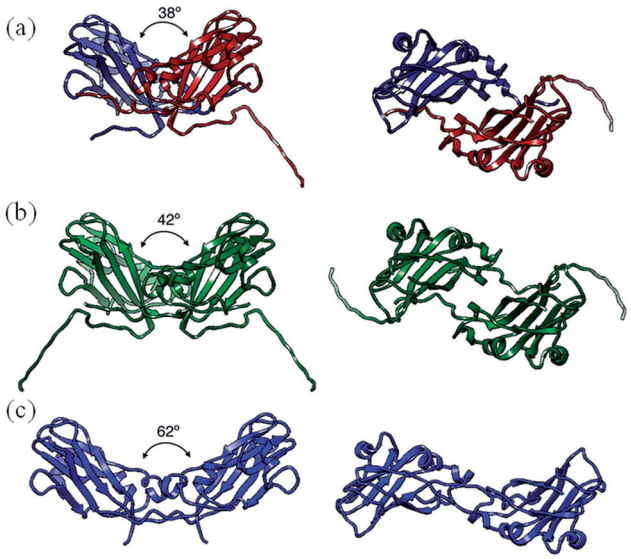

Fig. 6 Dihedral angles for CP dimers in ZnPc-loaded $T = 3$ and $T = 1$ VLP. (a) A–B and (b) C–C dimers in ZnPc-loaded $T = 3$ VLP. (c) A–A dimers in ZnPc-loaded $T = 1$ VLP. Side (left) and top (right) views. Hinge dihedral angles are indicated for the three CP dimer types.

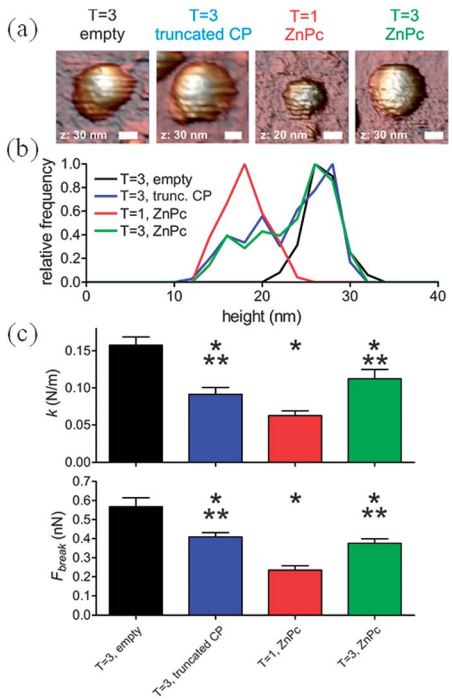

Fig. 7 (a) AFM images of CCMV-based VLP. Bars = 20 nm. Images are colored according to height, from dark-brown (low) to white (high), and maximum z is indicated. (b) Height distributions of CCMV-based VLP as determined from AFM images. (c) Mechanical properties of CCMV-based VLP. The spring constant (k) is shown in the top panel and the breaking force (F_{break}) in the bottom panel. Data are shown as mean ± SEM. Significance was tested by one-way ANOVA; $p < 0.0023$ for spring constant, $p < 0.0001$ for breaking force. Single asterisks (*) indicate $p < 0.01$ in Bonferroni-corrected t-testing between '$T = 3$, empty' and other particle types. Double asterisks (**) indicate $p < 0.01$ in Bonferroni-corrected t-testing between '$T = 1$, ZnPc' and other particle types.

compared them to empty capsids (sample **3**); to differentiate CP truncation from ZnPc encapsulation effects, empty capsids with truncated CP were included in the analysis (sample **4**). All VLP appeared as rounded particles in AFM imaging (Fig. 7a). Particle heights were consistent with $T = 1$ and $T = 3$ capsids, and with the mass distributions found by native MS. Sample **2** showed three populations of particles with different heights, whereas sample **1** was monodisperse, containing only VLP corresponding to $T = 1$ capsids (Fig. 7b).

We measured force–distance curves of the VLP (Fig. S6, ESI†). Spring constants and breaking forces for ZnPc-loaded $T = 1$ and $T = 3$ VLP were ~60% and 30% lower than those of empty $T = 3$ capsids with full-length CP (Fig. 7c). Empty $T = 3$ particles with truncated CP showed a similar 30% decrease in mechanical resilience. Based on these findings, we inferred that CP truncation reduces the mechanical resilience of ZnPc-loaded $T = 3$ VLP. ZnPc-loaded $T = 1$ VLP also showed markedly reduced stability compared to ZnPc-loaded $T = 3$ VLP, which can be ascribed to the structural differences between their protein cages. We postulate that the large difference in the hinge dihedral angle in $T = 1$ VLP CP dimers compared to $T = 3$ capsids determines their mechanical lability.

Implications of the ZnPc-loaded $T = 1$ VLP structure

In addition to the influence of the structures of ZnPc-loaded VLP on their mechanical behaviour, other properties of these assemblies are intimately related to their striking architectural features. The UV-Vis spectrum of the ZnPc-loaded $T = 3$ VLP (sample **2**) showed the absorption maximum at 635 nm, indicating ZnPc dimer formation as occurs in aqueous solutions (Fig. S1c and S5a, ESI†),[45,46] whereas the absorption maximum of ZnPc-loaded $T = 1$ VLP (sample **1**) was 613 nm (Fig. S1c, ESI†). We interpret these data based on our finding that the ZnPc forms nanospheres in $T = 1$ VLP. Size constriction of functional inorganic compounds to nanoscopic dimensions can provoke substantial changes in optical properties (*e.g.*, plasmonic effects in quantum dots and gold nanoparticles).[52] Although this behavior is uncommon for organic nanostructures, we observed a clear hypsochromic absorption shift (from 635 to 613 nm) as a result of the organization imposed on the ZnPc by $T = 1$ VLP.

Our findings suggest that to be packed as nanospheres, ZnPc molecules within $T = 1$ VLP are forced to self-assemble into long supramolecular stacks. Because the absorption shift is hypsochromic, the stacks are deduced to be type H (cofacial). We propose a model for this packaging, in which up to 18 ZnPc 10-mer stacks are fitted in the ZnPc density; stacks are parallel to the inner capsid wall in an arrangement reminiscent of an old-fashioned soccer ball (Fig. 8). These 180 ZnPc molecules would form a ~1.5 nm thick spherical shell, inside which a concentric ZnPc shell could form until the average of 250 ZnPc molecules per VLP is reached (as shown by MS analysis). In this model, ~3.0 to 3.5 nm thick ZnPc shells would produce a hollow nanosphere, as inferred from the cryo-EM 3DR radial density profile. Other ZnPc H-type stack arrangements such as radial stacks (see Fig. S5b, ESI†) can also be fitted, and thus should not be fully ruled out, although this would lead to greater electrostatic repulsion between negative charges of ZnPc stacks near the nanosphere core.

Our studies help to clarify the assembly mechanism of these ZnPc-loaded $T = 1$ VLP. Assembly of CCMV empty $T = 3$ capsids proceeds by adding CP dimers to a preformed pentameric nucleation center.[49] The kinetics of $T = 3$ capsid assembly differs when viral nucleic acid is present, presumably initiated by formation of an irregular nucleoprotein aggregate (similar to a reverse micelle), on whose surface additional CP subunits are assembled.[53] An analogous process might operate in CCMV-based VLP assembly at neutral pH, templated by polyanions such as gold nanoparticles coated with carboxylated PEG.[22,23] We hypothesize that ZnPc dimers can nucleate CP pentamer and hexamer formation. The greater curvature and smaller cavity of $T = 1$ capsids generated by addition of ZnPc dimer–CP pentamer complexes to the first pentameric nuclei would allow denser ZnPc packing, generating larger ZnPc stacks. ZnPc nanospheres would thus form gradually, driving assembly towards complete $T = 1$ capsids. Further study is needed to establish the precise structure of intermediate species.

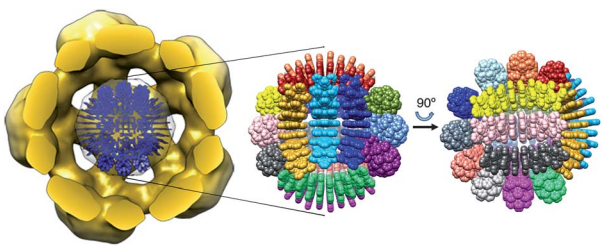

Fig. 8 Model of ZnPc organization within ZnPc-loaded $T = 1$ VLP, based on fitting supramolecular ZnPc stacks into the internal density of cryo-EM 3D-reconstructed particles. The scheme shows 10-mer ZnPc stacks (colors); only the outermost layer (180 ZnPc molecules) is shown. The ZnPc structure was modeled by molecular mechanics using Spartan'10 software.

Conclusions

ZnPc incorporation into protein cages composed of the CCMV capsid protein leads to a $T = 1$ VLP with unique structural features. CP assembly at neutral pH fosters ZnPc stack aggregation, which leads to formation of 10 nm ZnPc nanospheres. Such small, organized dye nanostructures, a consequence of capsid-imposed symmetry and size constraints, have not been described previously. Encapsulation of the ZnPc cargo produces substantial structural changes in the protein cage and alters its mechanical properties. To improve VLP stability for efficient PDT drug delivery, its mechanical properties must be characterized. There are also many optoelectronic applications of Pc dyes that are dependent on dye organization at the nanoscale level.[3–7] Multidisciplinary studies such as the one presented herein are thus necessary for implementing nanomedical and nanotechnological uses of these biohybrid materials.

Acknowledgements

We thank C Mark for editorial assistance. AE holds a Ramón y Cajal contract from the Spanish Ministry of Science and Innovation (MICINN). GJLW and WHR acknowledge the support of *Fundamenteel Onderzoek der Materie* (FOM) through the "Physics of the genome" program. This work was supported by the Spanish Ministry of Economy and Competitivity (MEC) and the MICINN (CTQ-2011-24187/BQU to TT and AE, and BFU2011-25902 to JRC), Consolider-Ingenio Nanociencia Molecular (CSD2007-00010 to TT and AE) and the Comunidad de Madrid (MADRISOLAR-2, S2009/PPQ/1533 to TT and AE).

Notes and references

1 *Handbook of Porphyrin Science*, ed. K. M. Kadish, K. M. Smith and R. Guilard, World Scientific, Singapore, 2013.
2 V. V. Roznyatovskiy, C.-H. Lee and J. L. Sessler, *Chem. Soc. Rev.*, 2013, **42**, 1921.
3 G. de la Torre, C. G. Claessens and T. Torres, *Chem. Commun.*, 2007, 2000.
4 F. Dumoulin, M. Durmus, V. Ahsen and T. Nyokong, *Coord. Chem. Rev.*, 2010, **254**, 2792.
5 J. Mack and N. Kobayashi, *Chem. Rev.*, 2011, **111**, 281.
6 G. Bottari, G. de la Torre, D. M. Guldi and T. Torres, *Chem. Rev.*, 2010, **110**, 6768.

7 C. G. Bezzu, M. Helliwell, J. E. Warren, D. R. Allan and N. B. McKeown, *Science*, 2010, **327**, 1627.
8 H. Kasai, H. S. Nalwa, H. Oikawa, S. Okada, H. Matsuda, N. Minami, A. Kakuta, K. Ono, A. Mukoh and H. Nakanishi, *Jpn. J. Appl. Phys.*, 1992, **31**, L1132.
9 X. C. Gong, T. Milic, C. Xu, J. D. Batteas and C. M. Drain, *J. Am. Chem. Soc.*, 2002, **124**, 14290.
10 S. Das, D. Bwambok, B. El-Zahab, J. Monk, S. L. de Rooy, S. Challa, M. Li, F. R. Hung, G. A. Baker and I. M. Warner, *Langmuir*, 2010, **26**, 12867.
11 C. Lu, S. Das, P. K. S. Magut, M. Li, B. El-Zahab and I. M. Warner, *Langmuir*, 2012, **28**, 14415.
12 S. L. de Rooy, S. Das, M. Li, B. El-Zahab, A. Jordan, R. Lodes, A. Weber, L. Chandler, G. A. Baker and I. M. Warner, *J. Phys. Chem. C*, 2012, **116**, 8251.
13 T. Douglas and M. Young, *Science*, 2006, **312**, 873.
14 A. de la Escosura, R. J. M. Nolte and J. J. L. M. Cornelissen, *J. Mater. Chem.*, 2009, **19**, 2274.
15 V. M. Rotello, *J. Mater. Chem.*, 2008, **18**, 3739.
16 Z. Liu, J. Qiao, Z. Niu and Q. Wang, *Chem. Soc. Rev.*, 2012, **41**, 6178.
17 Q. Wang, T. W. Lin, L. Tang, J. E. Johnson and M. G. Finn, *Angew. Chem., Int. Ed.*, 2002, **41**, 459.
18 L. S. Witus and M. B. Francis, *Acc. Chem. Res.*, 2011, **44**, 774.
19 N. Stephanopoulos and M. B. Francis, *Nat. Chem. Biol.*, 2011, **7**, 876.
20 M. A. Kostiainen, P. Hiekkataipale, A. Laiho, V. Lemieux, J. Seitsonen, J. Ruokolainen and P. Ceci, *Nat. Nanotechnol.*, 2013, **8**, 52.
21 T. Douglas and M. Young, *Nature*, 1998, **393**, 152.
22 J. Sun, C. DuFort, M.-C. Daniel, A. Murali, C. Chen, K. Gopinath, B. Stein, M. De, V. M. Rotello, A. Holzenburg, C. C. Kao and B. Dragnea, *Proc. Natl. Acad. Sci. U. S. A.*, 2007, **104**, 1354.
23 M.-C. Daniel, I. B. Tsvetkova, Z. T. Quinkert, A. Murali, M. De, V. M. Rotello, C. C. Kao and B. Dragnea, *ACS Nano*, 2010, **4**, 3853.
24 J. L. Lau, M. M. Baksh, J. D. Fiedler, S. D. Brown, A. Kussrow, D. J. Bornhop, P. Ordoukhanian and M. G. Finn, *ACS Nano*, 2012, **5**, 7722.
25 J. Lucon, S. Qazi, M. Uchida, G. J. Bedwell, B. LaFrance, P. E. Prevelige Jr and T. Douglas, *Nat. Chem.*, 2012, **4**, 781.
26 J. J. L. M. Cornelissen, *Nat. Chem.*, 2012, **4**, 775.
27 J. A. Speir, S. Munshi, G. J. Wang, T. S. Baker and J. E. Johnson, *Structure*, 1995, **3**, 63.
28 J. E. Johnson and J. A. Speir, *J. Mol. Biol.*, 1997, **269**, 665.
29 I. J. Minten, L. J. A. Hendriks, R. J. M. Nolte and J. J. L. M. Cornelissen, *J. Am. Chem. Soc.*, 2009, **131**, 17771.
30 M. Comellas-Aragones, H. Engelkamp, V. I. Claessen, N. Sommerdijk, A. E. Rowan, P. C. M. Christianen, J. C. Maan, B. J. M. Verduin, J. J. L. M. Cornelissen and R. J. M. Nolte, *Nat. Nanotechnol.*, 2007, **2**, 635.
31 I. J. Minten, V. I. Claessen, K. Blank, A. E. Rowan, R. J. M. Nolte and J. J. L. M. Cornelissen, *Chem. Sci.*, 2011, **2**, 358.
32 A. de la Escosura, M. Verwegen, F. D. Sikkema, M. Comellas-Aragones, A. Kirilyuk, T. Rasing, R. J. M. Nolte and J. J. L. M. Cornelissen, *Chem. Commun.*, 2008, 1542.
33 M. Kwak, I. J. Minten, D.-M. Anaya, A. J. Musser, M. Brasch, R. J. M. Nolte, K. Müllen, J. J. L. M. Cornelissen and A. Herrmann, *J. Am. Chem. Soc.*, 2010, **132**, 7834.
34 F. D. Sikkema, M. Comellas-Aragones, R. G. Fokkink, B. J. M. Verduin, J. J. L. M. Cornelissen and R. J. M. Nolte, *Org. Biomol. Chem.*, 2007, **5**, 54.
35 Y. F. Hu, R. Zandi, A. Anavitarte, C. M. Knobler and W. M. Gelbart, *Biophys. J.*, 2008, **94**, 1428.
36 M. Comellas-Aragones, A. de la Escosura, A. J. Dirks, A. van der Ham, A. Fuste-Cune, J. J. L. M. Cornelissen and R. J. M. Nolte, *Biomacromolecules*, 2009, **10**, 3141.
37 M. Brasch and J. J. L. M. Cornelissen, *Chem. Commun.*, 2012, **48**, 1446.
38 K. Burns, S. Mukherjee, T. Keef, J. M. Johnson and A. Zlotnick, *Biomacromolecules*, 2010, **11**, 439.
39 S. Mukherjee, C. M. Pfeifer, J. M. Johnson, J. Liu and A. Zlotnick, *J. Am. Chem. Soc.*, 2006, **128**, 2538.
40 A. de la Escosura, P. G. A. Janssen, A. P. H. J. Schenning, R. J. M. Nolte and J. J. L. M. Cornelissen, *Angew. Chem., Int. Ed.*, 2010, **49**, 5335.
41 B. C. Ng, S. T. Chan, J. Lin and S. H. Tolbert, *ACS Nano*, 2011, **5**, 7730.
42 L. Lavelle, M. Gingery, M. Phillips, W. M. Gelbart, C. M. Knobler, R. D. Cadena-Nava, J. R. Vega-Acosta, L. A. Pinedo-Torres and J. Ruiz-Garcia, *J. Phys. Chem. B*, 2009, **113**, 3813.
43 R. D. Cadena-Nava, Y. Hu, R. F. Garmann, B. C. Ng, A. N. Zelikin, C. M. Knobler and W. M. Gelbart, *J. Phys. Chem. B*, 2011, **115**, 2386.
44 M. B. van Eldijk, J. C. Y. Wang, I. J. Minten, A. Zlotnick, R. J. M. Nolte, J. J. L. M. Cornelissen and J. C. M. van Hest, *J. Am. Chem. Soc.*, 2012, **134**, 18506.
45 M. Brasch, A. de la Escosura, Y. Ma, C. Uetrecht, A. J. R. Heck, T. Torres and J. J. L. M. Cornelissen, *J. Am. Chem. Soc.*, 2011, **133**, 6878.
46 T. Nyokong, *Coord. Chem. Rev.*, 2007, **251**, 1707.
47 M. Comellas-Aragones, F. D. Sikkema, G. Delaittre, A. E. Terry, S. M. King, D. Visser, R. K. Heenan, R. J. M. Nolte, J. J. L. M. Cornelissen and M. C. Feiters, *Soft Matter*, 2011, **7**, 11380.
48 D. Willits, X. Zhao, N. Olson, T. S. Baker, A. Zlotnick, J. E. Johnson, T. Douglas and M. J. Young, *Virology*, 2003, **306**, 280.
49 J. H. Tang, J. M. Johnson, K. A. Dryden, M. J. Young, A. Zlotnick and J. E. Johnson, *J. Struct. Biol.*, 2006, **154**, 59.
50 H. J. Liu, C. X. Qu, J. E. Johnson and D. A. Case, *J. Struct. Biol.*, 2003, **142**, 356.
51 W. H. Roos, R. Bruinsma and G. J. L. Wuite, *Nat. Phys.*, 2010, **6**, 733.
52 M. B. Cortie and A. M. McDonagh, *Chem. Rev.*, 2011, **111**, 3713.
53 J. M. Johnson, D. A. Willits, M. J. Young and A. Zlotnick, *J. Mol. Biol.*, 2004, **335**, 455.